Power control strategies and network performance assessment for C+L+S multiband optical transport

JOURNAL OF
Optical Communications
and Networking

Power control strategies and network performance assessment for C+L+S multiband optical transport

Bruno Correia,[1,*] Rasoul Sadeghi,[1] Emanuele Virgillito,[1] Antonio Napoli,[2] Nelson Costa,[3] João Pedro,[3,4] and Vittorio Curri[1]

[1]DET, Politecnico di Torino, Corso Duca degli Abruzzi 24, Torino (TO) 10129, Italy
[2]Infinera, Sankt-Martinstr. 76, Munich, 81541, Germany
[3]Infinera Unipessoal Lda, Rua da Garagem 1, 2790-078 Carnaxide, Portugal
[4]Instituto de Telecomunicações, Instituto Superior Técnico, Av. Rovisco Pais 1, 1049-001 Lisboa, Portugal
*Corresponding author: bruno.dearaujo@polito.it

Received 7 January 2021; revised 22 March 2021; accepted 23 March 2021; published 13 April 2021 (Doc. ID 419293)

Spatial-division multiplexing (SDM) and band-division multiplexing (BDM) have emerged as solutions to expand the capacity of existing C-band wavelength-division multiplexing (WDM) optical systems and to deal with increasing traffic demands. An important difference between these two approaches is that BDM solutions enable data transmission over unused spectral bands of already-deployed optical fibers, whereas SDM solutions require the availability of additional fibers to replicate C-band WDM transmission. On the other hand, to properly design a multiband optical line system (OLS), the following fiber propagation effects have been taken into account in the analysis: (i) stimulated Raman scattering (SRS), which induces considerable power transfer among bands; (ii) frequency dependence of fiber parameters such as attenuation, dispersion, and nonlinear coefficients; and (iii) utilization of optical amplifiers with different doping materials, thus leading to different characteristics, e.g., in terms of noise figures. This work follows a two-step approach: First, we aim at maximizing and flattening the quality of transmission (QoT) when adding L- and L+S-bands to a traditional WDM OLS where only the C-band is deployed. This is achieved by applying a multiband optimized optical power control for BDM upgrades, which consists of setting a pre-tilt and power offset in the line amplifiers, thus achieving a considerable increase in QoT, both in average value and flatness. Second, the SDM approach is used as a benchmark for the BDM approach by assessing network performance on three network topologies with different geographical footprints. We show that, with optical power properly optimized, BDM may enable an increase in network traffic, slightly less than an SDM upgrade but still comparable, without requiring additional fiber cables.

https://doi.org/10.1364/JOCN.419293

1. INTRODUCTION

The capacity increase of optical networks is an important topic in the scientific community and industry. This topic has become particularly relevant due to challenges that have arisen from growing transport network traffic demands, which include the imminent deployment of 5G services [1] and the constant growth of IP traffic, cloud computing, and interconnections between data centers [2,3]. Most deployed optical transport networks operate using wavelength-division multiplexing (WDM) over a spectral window of approximately 4.8 THz in the C-band, with a transmission capacity of up to 38.4 Tb/s/fiber [4]. Further increasing network capacity requires solutions to be implemented, scaling the actual used technology (if possible), or applying news ones.

The most viable options to upgrade the available capacity of optical networks are (a) spatial-division multiplexing (SDM) [5,6], which can be implemented using multicore (MCF), multimode (MMF), or multiparallel (MPF) fibers, and (b) band-division multiplexing (BDM), which exploits a larger spectral portion of the fiber, aiming to enable transmission over the entire low-loss spectrum of optical fibers (e.g., ∼54 THz in ITU G.652.D fiber) [7]. Currently, among all SDM-based solutions, only MPF is commercially available, relying upon the availability of dark fibers or the deployment of new ones. This approach is realized by replicating the mature and cost-effective C-band line system technology. The remaining SDM solutions (e.g., MCF and MMF) have high potential to increase transmission capacity, but they require a complete transformation of the optical transport ecosystem, as they

imply the deployment of new fibers and devices. This requirement leads to high capital expenditures and complex logistics, making it unattractive for short- or midterm applications. Moreover, dedicated standards for MCFs have not yet been finalized, and commercial MCF solutions are not available, as this technology is mostly in the research phase [8]. On the other hand, BDM can maximize the return on investment of an already-deployed optical infrastructure, as it does not require immediate deployment of additional optical fibers, making it the most viable short-term solution to increase the capacity of optical networks.

Several works have evaluated the potential increase of transmission capacity through BDM techniques [7,9–16] using multiple spectral band combinations from the O- to L-band. Moreover, other investigations have addressed commercially available BDM solutions in the C+L transmission case [17–20], with up to 47 × 1.2 Tb/s super-channels in a WDM 200 GHz grid [21] for a total throughput of 56.4 Tb/s. These works focused on joint multiband power control for BDM systems in order to avoid the spectral tilt affecting the quality of transmission (QoT), considering both amplified spontaneous emission (ASE) and nonlinear interference (NLI) disturbances jointly with the stimulated Raman scattering (SRS), which plays a major role in multiband optical transmission [22,23]. The ASE noise and NLI, together with the SRS, are summed to define the generalized signal-to-noise ratio (GSNR), which can be effectively considered as the unique QoT parameter for a given lightpath [24] modeled as an additive white Gaussian-noise (AWGN) channel. The focus of [17] was on setting multiband power control strategies to maximize and flatten the GSNR over C+L line systems. In [18,19], the authors used the optimized power control to compute a network performance assessment by means of the statistical network assessment process (SNAP) [25].

Considering the low-loss window available on the extensively deployed ITU-T G.652D fibers, as WDM optical transport on the C+L-bands becomes more mature [16,21], the next step toward wider spectral window usage might be through activation of the S-band [26]. This would add up to ∼10 THz of additional spectrum; assuming a 50 GHz WDM grid, this would increase the channel count by ∼200 channels, roughly doubling the spectral availability of C+L line systems. In [22], a launch power optimization strategy for the C-, L-, and S-bands was performed, aiming to achieve a flat input power per band, taking into consideration the effects between bands, namely, the SRS. In this work, we optimize the power control for C+L+S multiband optical transmission, following the pre-tilt and offset strategy proposed in [18,19] for C+L-band scenarios. We consider two different spectral scenarios using the S-band, with 96 or 192 WDM channels able to be transported on the 50 GHz grid, with half of the S-band spectrum used for transmission in the first scenario. Then, supposing that optimized power control strategies are implemented within an optical control plane, we carry out a network performance assessment on three network topologies, considering uniform and nonuniform traffic models. Our analysis considers only completely transparent end-to-end lightpaths, without any regeneration capability in intermediary nodes. Analyzing the combination of different traffic and network characteristics, e.g., average nodal degree and average link distance, it is possible to evaluate the BDM capability to increase offered traffic in a broad range of network scenarios. Network performance that enables the BDM upgrade is benchmarked against the application of SDM, showing that BDM always approaches the traffic multiplication factor of the SDM.

The remainder of this paper is organized as follows. The QoT evaluation and the multiband power control strategy used in this work are described in Sections 2 and 3, respectively. In Section 4, we present the network performance assessment analysis. Next, we describe the adopted methodology in Section 5. In Section 6, the main results are presented and discussed, and the conclusions are outlined in Section 7.

2. LIGHTPATH QUALITY OF TRANSMISSION

In optical networks that employ dual-polarization WDM uncompensated coherent transmission systems, transparent lightpaths with a sufficient number of spans can be effectively modeled as additive Gaussian noise channels. Consequently, the QoT of an optical circuit can be estimated using the generalized signal-to-noise ratio, which includes the effect of additive Gaussian disturbances [23]. These are the ASE noise introduced by the optical amplifiers and the nonlinear interference due to the self- and cross-channel nonlinear crosstalk in fiber propagation. Additional GSNR impairments can be introduced by a reconfigurable optical add-drop multiplexer (ROADM) as the filtering penalty and Gaussian linear cross-talk. These effects are not considered in our analysis, being strongly related to the ROADM architecture. In this work, we assume a disaggregated abstraction of the physical layer [27,28], in which each network element is considered to introduce a gain or loss and some amount of Gaussian disturbance, i.e., the ASE noise by arising from the amplifiers and the NLI arising from propagation. Hence, the GSNR for the ith channel under test is defined as

$$\mathrm{GSNR}_i = \frac{P_{S,i}}{P_{\mathrm{ASE},i} + P_{\mathrm{NLI},i}} = \left(\mathrm{OSNR}_i^{-1} + \mathrm{SNR}_{\mathrm{NL},i}^{-1}\right)^{-1}, \tag{1}$$

where the optical signal-to-noise ratio is $\mathrm{OSNR}_i = P_{S,i}/P_{\mathrm{ASE},i}$ and the nonlinear signal-to-noise ratio is $\mathrm{SNR}_{\mathrm{NL},i} = P_{S,i}/P_{\mathrm{NLI},i}$ with $P_{S,i}$ being the signal input power of the ith channel. $P_{\mathrm{ASE},i}$ and $P_{\mathrm{NLI},i}$ are the amounts of ASE noise and NLI accumulated over the lightpath propagation by the ith channel. In this work, for the GSNR evaluation, we use the QoT estimator (QoT-E) of the GNPy open-source project [29,30]. The amount of ASE noise introduced by each amplifier is computed by knowing its gain (G) and noise figure (NF):

$$P_{\mathrm{ASE}}(f) = hf\mathrm{NF}(f)G(f)B_{\mathrm{ref}}, \tag{2}$$

where h is Planck's constant, f is the frequency of the channel under test, and B_{ref} is the reference bandwidth. Noise figures on different bands are set according to commercial (C+L-bands) or prototype (S-band) lumped doped-fiber amplifiers. The amount of NLI P_{NLI} introduced by each fiber span is computed according to the generalized GN model [23], which

considers the fundamental interaction between NLI generation and SRS and which dominates power optimization in multiband line systems. Therefore, the QoT-E includes an accurate solver for the SRS ordinary differential equation (ODE) [31] in order to accurately define the spectral/spatial evolution of power over each fiber span. The speed of the NLI evaluation is increased by computing only the self- and cross-channel NLI contributions, since the multichannel NLI contributions are always negligible in practical scenarios [29]. Besides the SRS effect, the frequency dependence of loss and dispersion are accurately considered to properly capture the multiband effects and trade-offs.

3. MULTIBAND POWER CONTROL STRATEGIES

Propagation of optical signals in the glass is always affected by the SRS, i.e., a nonlinear effect that induces a power transfer from higher to lower frequencies. As a consequence, higher frequencies suffer a power depletion that enhances their losses, whereas lower frequencies are pumped, showing a reduction of the intrinsic fiber loss [20]. When considering the effect of SRS together with the ASE noise and NLI generation, it can be deduced that higher frequencies are more affected by the ASE noise because of the higher loss due to SRS and, consequently, the higher gain required to recover this loss; however, they are affected less by the NLI whose generation is mitigated by the SRS-induced power depletion. The opposite occurs for lower frequencies. SRS is a wideband phenomenon with maximum efficiency at ∼13 THz spectral down-spacing, so it is relevant but weak for C-band-only transmission, where it induces a spectral tilt that can be compensated for, e.g., by gain-flattening filters. Conversely, in networks using multiband systems, where transmission approaches 13 THz of continuous spectral occupation (such as for C+L-band line systems) or exceeds it as for C+L+S-band line systems, the SRS becomes the dominant effect in power control.

The power control unit (PCU) for line systems is part of the control plane and sets the amplifier working points to optimize performance and maximize GSNR for each WDM wavelength. We assume that a multiband optical system is built by a series of bands where the components, in particular the optical amplifiers, are optimized per band as proposed in [7]. In this scenario, the PCU must operate simultaneously on all amplifiers within an optical line system (OLS) to optimize the transmission, as illustrated in Fig. 1, which depicts a PCU controlling the amplifier working points for each spectral band on an individual basis.

With a disaggregated approach, the power optimization can be performed following a span-by-span strategy [32,33] using the local optimization global optimization (LOGO) algorithm as starting point, which is based on obtaining QoT maximization under the assumption of full link spectral loading [34]. In this work, we follow such an approach by operating on the two parameters, i.e., the average gain/output power and the related tilt, which can be typically set in commercial amplifiers. Therefore, the aim of an optimized PCU is to jointly set the average output power and tilt per band in order to maximize and flatten the per-band GSNR and, consequently, the deployable capacity [17]. The optimization procedure for a single

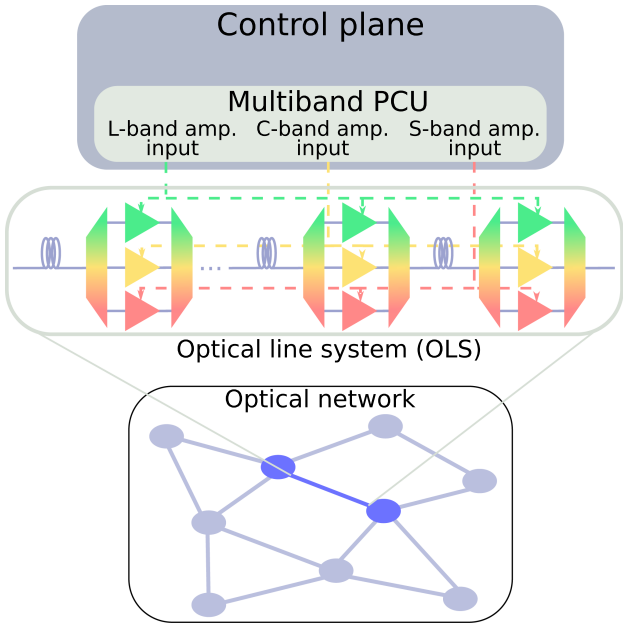

Fig. 1. Illustration of the application of a PCU to control multiple multiband amplifiers in an OLS.

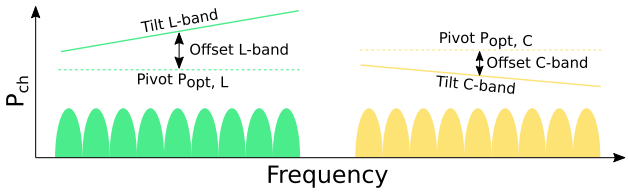

Fig. 2. Illustration of the tilt and offset strategy for the C+L-band transmission scenario.

fully loaded span, composed by a fiber and an amplifier, starts by setting a flat launch power at the per-band optimum [33], neglecting frequency variations and SRS; then, per-band power offset and tilt are varied to obtain the optimal solution. This strategy is illustrated in Fig. 2. Here, the L-band channels (green) are launched into the optical fiber with a flat power, with positive power offset and tilt added (which defines the slope of the launch power), measured in dB/THz. On the other hand, the C-band channels (yellow) are launched into the optical fiber with a negative power offset and tilt, which corresponds to a decrease in power level along this spectral region. To set the optimal per-band offset and tilt, we performed a brute-force computation, where all combinations were analyzed, and the GSNR was evaluated for each scenario by running GNPy. The described approach has previously been investigated for C- and C+L-band scenarios in [18,19]; here, we expanded it to include the S-band. Results of the optimization are then used as a hypothesis for operational settings in the network control plane, and the network topology can be consequently abstracted for physical-layer-aware networking analyses [27]. Such network abstraction is then used for network performance assessment to derive the impact on the networking performance of multiband provisioning with optimized power control. The power optimization procedure

is also applied to the C-only scenario to perform networking analyses in the case of SDM applications that are used to benchmark the BDM approach.

4. NETWORK PERFORMANCE ASSESSMENT

To analyze how the different physical layer optical transport solutions have an impact on the overall network performance, we exploited SNAP [25], which operates on the physical layer abstraction of the network under test, based on the GSNR degradation introduced by each network element [27], and statistically test the network progressive load with different traffic models. Lightpaths are allocated according to the defined routing and wavelength assignment (RWA) algorithm and transceiver characteristics. Networking metrics are obtained statistically by performing Monte Carlo analysis. In this work, to explore the fundamental limitations and determine the capacity limits for the BDM upgrade, we assume the presence of ideal flexible transceivers that are able to continuously adapt the bit-rate to the available lightpath GSNR. This framework can handle two types of traffic models, which result in two different types of analysis: (a) given-traffic analysis, in which all traffic (in number of lightpaths or bit-rate) between all nodes in the network is known in advance and (b) progressive traffic analysis, in which the model generates requests evolving progressively until a predefined stop criterion, such as the total amount of requests or the total number of blocked requests, is reached. The latter analysis intends to stress the network and to obtain, besides the static metric at the end of the simulation, a progressive metric that represents the loading evolution of the network. For progressive traffic analysis, SNAP can handle different types of traffic distributions by changing the joint probability density function (JPDF), which is responsible for determining the frequency of requests between each node pair in the network. SNAP can produce outputs such as the bit-rate of each lightpath allocated in the network as well as the bit-rate average per lightpath, details about spectral occupation, number of blocked requests by nodes or links, among other metrics. In this work, we compare the different scenarios referring to the blocking probability (BP) versus the overall allocated traffic. Then, given the target BP $= 10^{-2}$, we also focus on congestion on ROADM-to-ROADM connections.

5. ANALYSIS

In this work, for all network topologies, we consider every fiber span in the amplified lines to have identical lengths and fiber types of 75 km and ITU-T G.652D standard single-mode fiber (SSMF), respectively. We assume lumped amplification for full loss recovery. For channels in the C- and L-bands, we consider commercially available erbium-doped fiber amplifiers (EDFAs), and in the S-band we consider channels amplified with a benchtop thulium-doped fiber amplifier (TDFA) with the characteristics reported in [35]. As amplifiers for the S-band remain unavailable commercially, in this work we use the noise figure (NF) values of the aforementioned benchtop amplifier. Figure 3 shows this NF, which presents an average value of ∼6.5 dB. For C- and L-band amplifiers, the NF average is ∼4.25 and ∼4.68 dB, respectively, as displayed in Fig. 3. It can be noted that the noise figure profile for the TDFA presents a significantly lower performance compared with the commercial EDFAs. Moreover, it assumes a constant NF profile regarding amplifier power and tilt or spectral configuration. Our analysis, closely related to the fixed NF profiles used, intends to show that it is possible to achieve acceptable performance in terms of QoT and delivered traffic with the current development state of those amplifiers. Each band operates upon the ITU-T 50 GHz WDM grid with transceivers setting a symbol rate of 32 GBaud, with guard bands between adjacent bands having a minimum width of 500 GHz. For the C- and L-bands we use 96 channels each, combined with two different S-band channel arrangements: 96 channels adjacent to the C-band (respecting the guard band distance) and the use of the entire S-band, corresponding to 192 channels. Initially, the launch power per channel is set to −2.1, −1.99, and −2.0 dBm for the C-, L-, and S-bands, respectively.

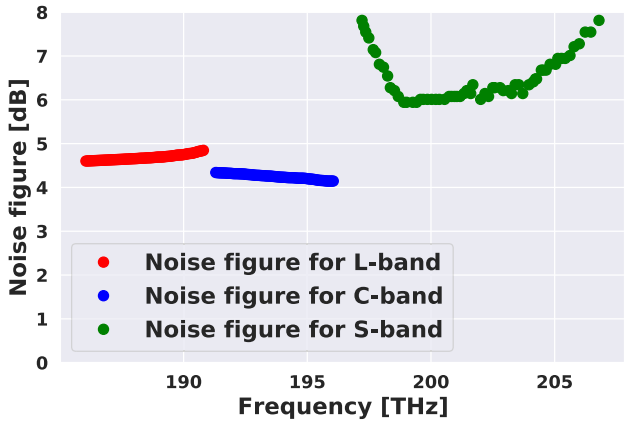

Fig. 3. Amplifier noise figures for all spectral bands used in BDM analysis.

In order to set parameters in a multiband power control scenario, a brute-force approach was considered, with a range of pre-tilts and offsets dependent upon the bands under consideration. For C and C+L scenarios, the range of pre-tilting varies from −0.5 to 0.5 dB/THz, with a step size of 0.1 dB/THz. The offsets vary from −1.0 to 2.0 dB and −2.0 to 1.0 dB for the C- and L-band scenarios, respectively, both with a step size of 1 dB, resulting in 44 combinations for the C-band and almost 2000 combinations for the C+L band case. In the two cases where the S-band is added, different sets were used in order to avoid an excessive number of combinations. For the C- and L-bands, the pre-tilt varies from −0.5 to 0.5 dB/THz with a step size of 0.2 dB/THz, along with a flat tilt value and an offset varying from −1.0 to 1.0 dB. For the S-band, the pre-tilt varies from 0.0 to 3.0 dB for both cases (96 and 192 in the S-band), with all scenarios having with a step size of 1.0 dB, performing ∼12,000 combinations for each scenario. The NLI contribution is computed for five channels in each band containing 96 channels and for 10 channels in the S-band case with 192 channels, in order to increase the speed of the algorithm. The central channel of the spectral band is computed, and a frequency distance of around 1 THz is used for the other computed channels. For the remaining channels, their GSNRs are interpolated from those that have already been computed, following the same procedure in [18].

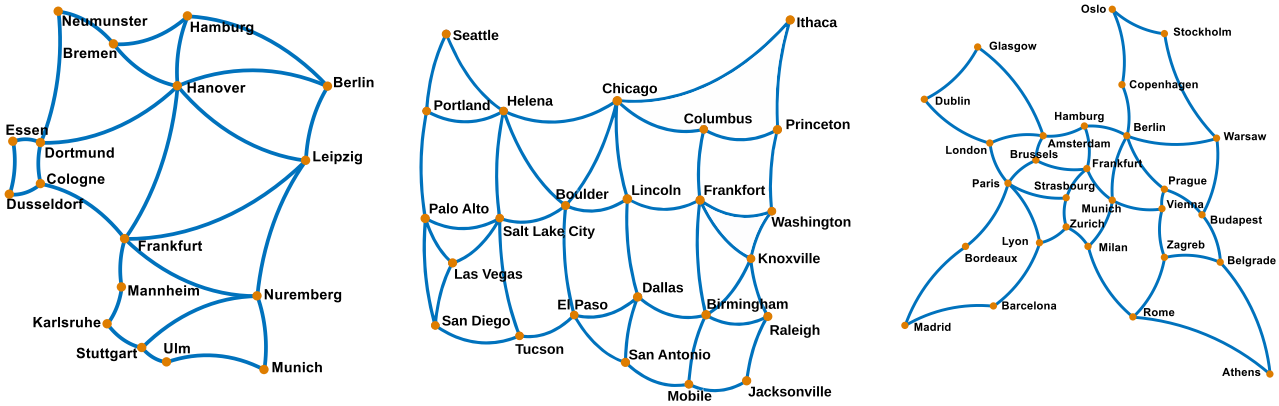

(a) (b) (c)

Fig. 4. Reference networks analyzed: (a) German, (b) US-NET, and (c) COST topologies.

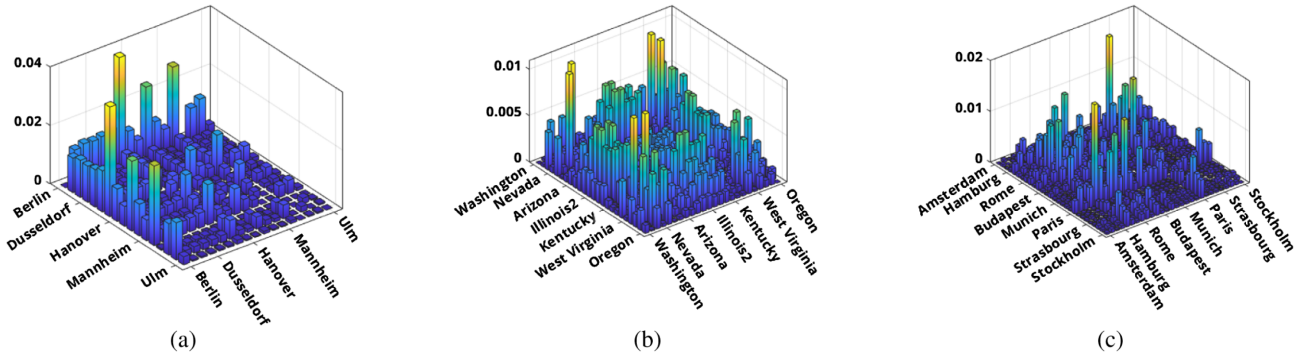

(a) (b) (c)

Fig. 5. Nonuniform population-based JPDF for (a) German, (b) US-NET, and (c) COST topologies.

Three network topologies, shown in Fig. 4, are considered to statistically assess the network performance:

- The German network shown in Fig. 4(a) is composed of 17 optical nodes and 26 edges with an average nodal degree of 3.1, average distance between nodes of 207 km, and maximum link length of 300 km.
- The US-NET topology shown in Fig. 4(b) consists of 24 optical nodes and 43 edges, with an average nodal degree of 3.6, average distance between nodes of 308 km, and maximum link length of 525 km.
- The European COST network shown in Fig. 4(c) has 28 nodes and 41 edges, an average nodal degree of 2.93, average distance between nodes of 637 km, and maximum link length of 1125 km.

Regarding the parameters required by the SNAP to obtain stable networking metrics, $N_{\mathrm{MC}} = 30{,}000$ iterations were used for the Monte Carlo algorithm for the German topology and $N_{\mathrm{MC}} = 20{,}000$ for the US-NET and COST topologies, the latter being larger networks and necessitating a reduction in the number of iterations in order to minimize computational effort. A k-shortest path algorithm is used for routing, with $k = 15$, and first-fit (FF) applied for a wavelength assignment (WA) in a progressive traffic analysis to obtain both dynamic and static metrics [25]. Particularly for the SDM case, the WA tries all channels of the first fiber set, e.g., C-band 1, before it tries to allocate in the second set, also following the FF. Lightpath requests are progressively generated for each Monte Carlo run, exploring two scenarios with statistical traffic models that are characterized by different JPDFs: (1) a uniform JPDF where, at each connection request, the probability is the same for any source and destination and (2) a distribution based on population [18], denoted by the nonuniform case within this work. The nonuniform JPDF is presented in Fig. 5, in which requests between optical nodes in cities with a higher population have a larger probability to occur than between nodes placed in less-populated cities.

Formally, the probabilities, $P(s, d)$, of a source-destination node pair to be chosen in the uniform and nonuniform JPDFs, respectively, are given by

$$P(s, d) = \frac{1}{N(N-1)}, \tag{3}$$

$$P(s, d) = \frac{pop_s \cdot pop_d}{\sum_{(i,j)\in A} pop_i \cdot pop_j}, \tag{4}$$

in which N is the total number of nodes in the considered network topology, pop_x is the population of the city geographically located in node x, and $(i, j) \in A$ represents all possible source-destination nodes pairs (i, j) in the network topology A. The network performance is evaluated for the multiband amplifier power control, with the optimal GSNR profile obtained through the brute-force approach previously described. The

bit-rate over each lightpath (LP) is deployed assuming ideal elastic transceivers that deliver the bit-rate according to the available GSNR, as per the Shannon law. Thus, we focus on exploring the fundamental transmission limitations within the considered network topology, without being limited by a specific transceiver implementation.

6. RESULTS

In this section, we present the results obtained for the three considered network topologies. We start with the multiband power optimization and follow with the networking results. To ensure a fair benchmark of the multiband results, we compare BDM against SDM network performance with SNAP analyses, assuming SDM deployment using multiple fibers within the C-band on the same overall available spectrum. For SDM, we assume a core continuity constraint (CCC), where each LP must be allocated in the same fiber from the source to the destination node, according to the switching technique [5,6]. This option is preferred due to the amount of fiber pairs that will be multiplied, by three and four, to compare with the BDM approach using C+L+S. Reference [36] shows that this scalability of ROADMs' architecture can significantly increase insertion losses, footprint, and costs in such cases.

A. Transmission

First, the transmission QoT is evaluated. Figure 6 presents the optimized per-span GSNR profiles for the four multiband scenarios: C-band only (reference scenario) with 96 channels, C+L-band with 192 channels, and C+L+S-band cases (288 and 384 channels). Each case refers to the tilt and offset values reported in Table 1, obtained via the brute-force optimization described in Section 5. For the C-band-only deployment case (blue curves), the average per-span GSNR in the WDM comb of 96 channels is 30.5 dB. If we activate the L-band with an additional 96 channels (red curves) using a multiband power controller, the per-span average GSNR is 30.3 and 30.5 dB for C- and L-bands, respectively. Thus, C+L-band BDM shows a penalty of only 0.2 dB with respect to doubling the C-band-only transmission capacity. Even with this decrease, the launch power strategy is able to deliver an almost flat GSNR profile for both bands. When we activate an additional 96 channels in the S-band, creating a C+L+S-band BDM line system of 288 WDM channels (green curves), the optimal multiband power control guarantees an average per-span GSNR of 30.1, 31.0, and 26.8 dB for C-, L-, and S-bands, respectively. Within the C+L+S-band BDM implementation, the C-band experiences an additional yet limited average GSNR penalty of 0.2 dB per-span with respect to the C+L-band case, while the L-band benefits from SRS pumping into the lowest spectrally located channels, thereby slightly improving its GSNR. The 96 channels on the S-band present a poorer GSNR with respect to the other bands. This is mainly caused by the SRS and by the larger NF of the considered S-band amplifier. As the overall penalty of the S-band is limited to 4 dB, a reasonable transmission capacity is also enabled within this band, along with a limited perturbation on the C+L-band transmission performance. Observing the per-band GSNR flatness, we note

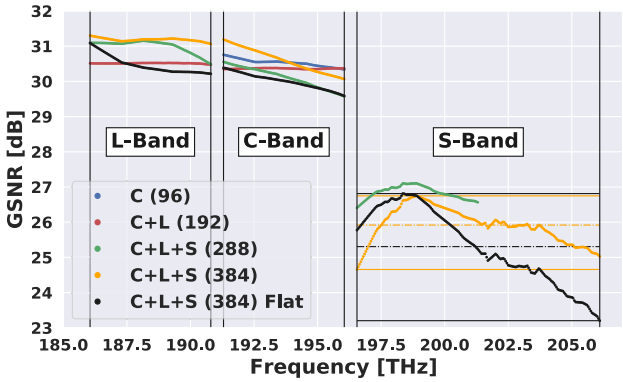

Fig. 6. 75 km fiber span GSNR versus frequency for all analyzed scenarios, maximum and minimum GSNR for the S-band (lines), and average GSNR (dashed lines) for the S-band, comparing launch power control with flat input powers.

Table 1. Optimum Launch Power Tilts and Offsets per Band for the C-, C+L-, and Both C+L+S-Band Transmission Cases

Bands	Pre-Tilts [dB/THz]			Offsets [dB]		
(No. of Channels)	L	C	S	L	C	S
C (96)	–	−0.5	–	–	0.0	–
C+L (192)	0.3	0.4	–	−2.0	−1.0	–
C+L+S (288)	−0.5	0.5	0.1	−1.0	−1.0	2.0
C+L+S (384)	−0.5	0.5	0.5	−1.0	−1.0	0.0

a worse performance with respect to the C+L-band case, but the difference between the maximum and minimum per-band GSNR is confined within 1 dB.

Finally, when we activate the entire S-band with 192 channels (orange curves) deploying a C+L+S-band WDM multiband line system, the optimal multiband power control ensures an average per-span GSNR of 30.6, 31.2, and 25.9 dB for the C-, L-, and S-band, respectively. In this case, we obtain the spectral availability of four C-band-only line systems. The transmission capacity of the 192 lower-frequency channels presents slightly larger QoT than the amount guaranteed by the two C-band-only line systems, thanks to the SRS pumping enabled by the S-band channels. For the additional 192 available channels in the S-band, the average GSNR is ∼ dB smaller. Nevertheless, this value can still guarantee good transmission capacity with 25.9 dB GSNR per span. With respect to the GSNR flatness, this last scenario shows an excellent value for this parameter of ∼0.1 dB in the L-band and ∼1.1 dB in the C-band with most of the values exceeding the C+L-band case. For the S-band, the flatness exceeds 2 dB in the 96 lower-frequency channels, while it is about 1 dB for the remaining 96 higher-frequency channels.

We also compared the multiband power control strategy with the flat spectrum power control, i.e., the LOGO strategy, independently on each band for the C+L+S-band BDM with 384 channels in total. We focus on the difference in the S-band to show the benefits of the proposed multiband power control strategy with respect to the LOGO. Referring to the yellow and black horizontal lines of Fig. 6, added to the S-band part, we show the minimum, maximum, and average (dashed lines)

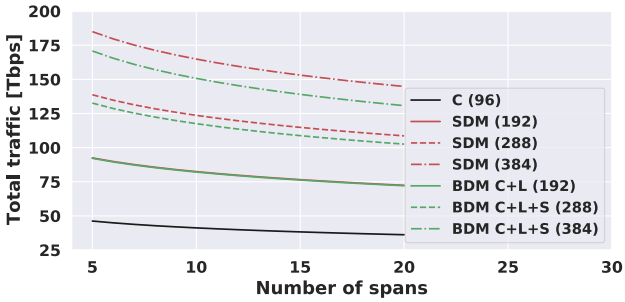

Fig. 7. Total allocated traffic versus number of fiber spans for all upgrade scenarios.

GSNR. We also highlight that the multiband power control enables a gain of 0.6 dB in the average GSNR and a flatness improvement of 1.5 dB with respect to the LOGO strategy only. Moving to the C- and L-band, the proposed method increases the average GSNR by 0.6 dB for the C-band and 0.7 dB for the L-band, with the L-band delivering an almost flat QoT. From a network management point of view, GSNR flatness is as important as the maximization of the average value, as it enables a larger set of wavelengths with equivalent performance, which simplifies the RWA algorithms and can reduce the impact of the wavelength continuity constraint in traffic allocation.

In order to assess the impact of the different upgrades in an OLS using the GSNR profile found by the power optimization, in Fig. 7 we present the allocated traffic with the increase of span numbers. For 10 spans, the capacity delivered by the C-band only case is 41.2 Tbps with SDM delivering two, three, and four times more for each scenario tested (82.4, 123.6, and 164.8 Tbps). With BDM upgrade, also for 10 spans, we obtained 82, 117, and 150 Tbps for all BDM scenarios (192, 288, and 384 channels). For the Shannon limit, used to determine the allocated traffic, doubling the channels is almost the same for the two upgrades (BDM/SDM), while the differences achieved around 6% and 9% for three and four times more channels, respectively, with SDM outperforming BDM. These results show the delivered traffic degradation due to the lower QoT profile of the BDM upgrade, serving as a reference to evaluate if the impact in a network scenario follows the same behavior.

B. Networking

The optimized transmission results are subsequently used to carry out network-level analyses, with the GSNR values for each WDM channel used to create the topological graph that is weighted by the GSNR degradation [27] in order to implement the SNAP. As the GSNR profiles presented in Section 6.A are obtained for a fully loaded span, and the network analysis is performed for progressive traffic, we assume a network with optical noise-loading capability, i.e., ROAMDs emulating fully loaded OLSs, being able to maintain the QoT levels with minimum changes compared with transmitted modulated signals. For all three network topologies reported in Fig. 4, a different BDM solution for WDM transmission is assumed, with the C-band-only scenario serving as a reference. For each case, SNAP is applied to uniform and nonuniform traffic models for the BDM and SDM cases, with the same spectral availability. Hereafter, we compare (i) the C+L BDM to the SDM 2×, (ii) the C+L+S-band (96) BDM to the SDM 3×, and finally (iii) the C+L+S-band (192) BDM to the SDM 4×. Results are displayed as a statistical average over the Monte Carlo runs of the BP versus total progressively allocated traffic, for each BDM and equivalent SDM scenario and for both traffic models. Taking $BP = 10^{-2}$ as a reference, the traffic values are considered in order to calculate the enabled traffic multiplication factor, which is used to fairly compare the different transmission solutions.

We comment on the networking results starting from the German topology, whose results are displayed in Fig. 8. Figures 8(a) and 8(b) plot BP versus the progressively total allocated traffic for the considered BDM and SDM solutions for uniform and nonuniform traffic models, respectively. In Fig. 8(a), for the German topology and uniform traffic model, for $BP = 10^{-2}$, we read 268 Tbps of total allocated traffic for the reference C-band-only case (black curve), while, using the BDM upgrade (green curves), we obtain ∼{568, 867, 1149} Tbps of total allocated traffic for the C+L-band, C+L+S-band (288), and C+L+S-band (384), respectively. For the equivalent reference C-band SDM solutions (red curves) based on two, three, and four fibers, we note only slightly larger values for the total allocated traffic, precisely: ∼{570, 879, 1187} Tbps, respectively. Similar behavior can be observed in Fig. 8(b) for the nonuniform traffic model. In general, this network topology seems to be well designed for a traffic model proportional to the population in the urban areas where each ROADM node is located; as with a nonuniform traffic model, the deployed total traffic is always larger than for the uniform case. The larger difference in allocated traffic is obtained comparing SDM with four fibers, with 1527 Tbps, and C+L+S (384), with 1445 Tbps. All results for the German topology are summarized, for comparison, in Fig. 8(c). Here, we report the values of total allocated traffic at $BP = 10^{-2}$ for all the considered BDM and corresponding SDM solutions. The green bars refer to the nonuniform traffic model, the red ones to uniform traffic. Besides the traffic values, the allocated traffic multiplication factors are displayed, taking as reference the C-band-only scenario. We observe that the nonuniform traffic always exceeds the uniform traffic for BDM and SDM solutions with a quite constant proportionality. For only the case of nonuniform traffic does the BDM case for the cardinality of 4 reach only 3.97 of the multiplication factor. As previously stated, such behavior is enabled by a topology well-tailored to this traffic model. Moving to analyze the BDM/SDM upgrade, we note that both solutions enable a traffic multiplication factor always exceeding the BDM/SDM cardinality. Comparing the BDM to the SDM solution, we observe that the reference SDM outperforms BDM always by less than 3%, confirming that multiband transmission can be a viable solution to expand the network traffic capacity without depending on new fiber structure or unused dark fibers.

Figure 9 presents the results for the US-NET topology with the C-band case providing 410 Tbps of total allocated traffic for $BP = 10^{-2}$ with uniform JPDF as the traffic model, as shown in Fig. 9(a). For the same JPDF and BP, the BDM upgrade provides total allocated traffic of

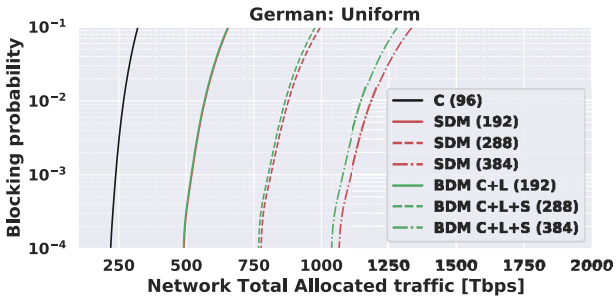

(a)

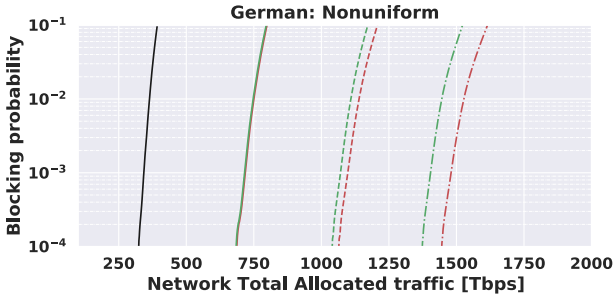

(b)

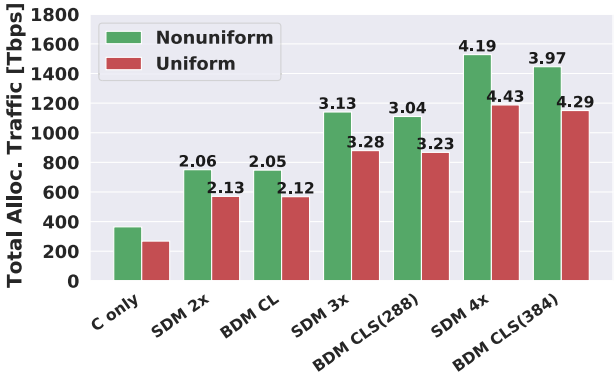

(c)

Fig. 8. Network performance results for the German topology. Total allocated traffic versus BP with (a) uniform and (b) nonuniform JPDFs and (c) total allocated traffic multiplicative factor for $BP = 10^{-2}$.

~{835, 1244, 1630} Tbps for the C+L-band, C+L+S-band (288), and C+L+S-band (384) cases, respectively. The SDM upgrade allocates more traffic in all considered scenarios, achieving ~{839, 1267, 1700} Tbps for C-band upgrades with two, three, and four fibers, respectively. Unlike the German topology, the traffic model based on population, applied to the US-NET, delivered less total traffic than the uniform case, as presented in Fig. 9(b). This can be explained by the topology characteristics, in which the most populated cities, where the ROADMs are located, are at the extremes of the network topology (east and west coasts), demanding ultra-long connections with higher frequency than with the uniform traffic distribution. At $BP = 10^{-2}$, the maximum capacity upgrade using BDM, obtained with four fibers, is 1405 Tbps, and, using SDM, using 384 channels, it is 1352 Tbps. It can be noted by the multiplicative factor reported in Fig. 9(c) that both upgrade scenarios using BDM more than double, triple, and quadruple the capacity for the two considered traffic models, with the highest difference in allocated traffic achieving ~3.8%, compared with SDM.

Finally, we present the results for the COST topology shown in Fig. 10. In Fig. 10(a), we report the results of allocated traffic for a uniform JPDF, with values for $BP = 10^{-2}$ of ~{260, 543, 816, 1072} Tbps for BDM using C-only, C+L-band, C+L+S-band (288), and C+L+S-band (384), respectively, and ~{547, 836, 1131} Tbps for SDM solutions using two, three, and four fibers, respectively. Regarding the nonuniform JPDF traffic model presented in Fig. 10(b) for the same BP, the maximum difference between SDM and BDM is approximately 50 Tbps. The multiplicative factor of this topology for both traffic JPDFs is shown in Fig. 10(c) and presents almost the same behavior as the ones observed with the previous topologies. In particular, only BDM C+L+S-band with 384 channels does not overcome the proportional increase of total allocated traffic compared with the reference C-band only case.

All three analyzed topologies, with the two traffic models, as shown in Figs. 8–10, present the same behavior of a small increase in the difference of allocated traffic between the BDM and the correspondent SDM technique as we increase the cardinality upgrade. The results are summarized in Table 2, which shows the allocated traffic multiplicative factors for all combinations of topology, upgrade scenario, and traffic JPDF. Note that the FF spectrum allocation policy used in this work prioritizes the channels with lower frequencies and leaves the higher-frequency channels to be used when the network is more loaded, which are the channels with the lower QoT levels. It can also be seen in Table 2 that the BDM technique enables an increase in the allocated traffic proportional to the cardinality upgrade in almost all cases, indicating that BDM is a viable option in a network-upgrade scenario in terms of

Table 2. Allocated Traffic Multiplicative Factors (C-Only as a Reference) of the German, US-NET, and COST Topologies for All Upgrade Scenarios and Traffic Distributions with $BP = 10^{-2}$

Topology	German		US-NET		COST	
Upgrade	Uniform	Nonuniform	Uniform	Nonuniform	Uniform	Nonuniform
SDM 2×	2.13	2.06	2.04	2.06	2.1	2.05
C+L	2.12	2.05	2.03	2.05	2.09	2.04
SDM 3×	3.28	3.13	3.09	3.1	3.21	3.09
C+L+S (288)	3.23	3.04	3.03	3.05	3.13	3.02
SDM 4×	4.43	4.19	4.14	4.16	4.34	4.13
C+L+S (384)	4.29	3.97	3.97	4.0	4.11	3.93

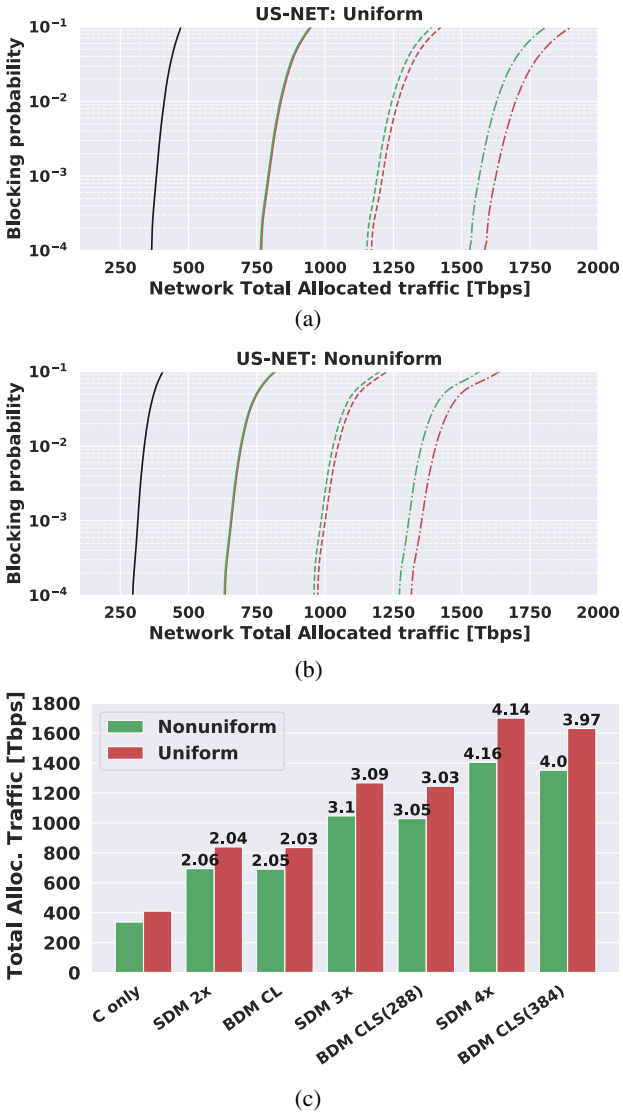

Fig. 9. Network performance results for the US-NET topology. Total allocated traffic versus BP with (a) uniform and (b) nonuniform JPDFs and (c) total allocated traffic multiplicative factors for $BP = 10^{-2}$.

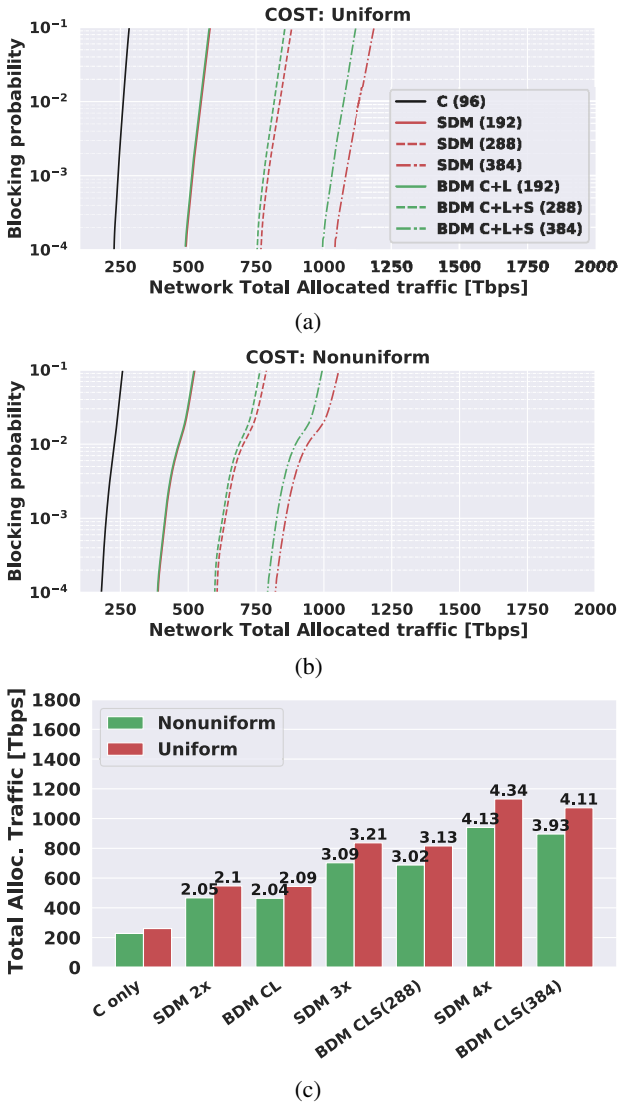

Fig. 10. Network performance results for the COST topology. Total allocated traffic versus BP with (a) uniform and (b) nonuniform JPDFs and (c) total allocated traffic multiplicative factor for $BP = 10^{-2}$.

delivered traffic. Moreover, the randomness of the traffic distribution can explain why the multiplicative factors can exceed the cardinality upgrade.

As a final result, we show in Fig. 11 the link congestion for the three topologies at $BP = 10^{-2}$, for the reference C-band scenario. These results highlight issues with the topology that can be solved by the selected upgrades. For the German topology [Fig. 11(a)], seven (uniform case) and nine (nonuniform case) out of 26 links present more than 80% of occupancy, while nine (uniform case) and eight (nonuniform case) links show less than 40% of usage. Results for the US-NET topology are displayed in Fig. 11(b) showing seven (uniform case) and eight (nonuniform case) out of 43 links presenting more than 80% of occupancy and 15 (uniform case) and 17 (nonuniform case) links with less than 40% of usage. For the COST topology, as shown in Fig. 11(b), seven (uniform case) and four (nonuniform case) out of 41 links present more than 80% of occupancy, while 15 (uniform case) and 21 (nonuniform case) links show less than 40% of usage. These plots provide additional insights with respect to the aggregated results of BP versus allocated traffic. The German topology, mostly when loaded with the nonuniform traffic model, shows >80% usage on about one-third of the available links; for the other topologies, only one-sixth of the total available links reaches more than 80% of usage. This is caused by the larger geographical footprint of the US-NET and COST topologies, which include several regional areas with large requests for intraregional traffic. Consequently, the overall network blocking is limited by congestion in those regional areas. To overcome this issue, the application of BDM on selected links may be largely beneficial for the overall network traffic. Specifically, we could envision the exploitation of the poorer QoT S-band for intraregional traffic and C+L bands for interregional long-reach traffic.

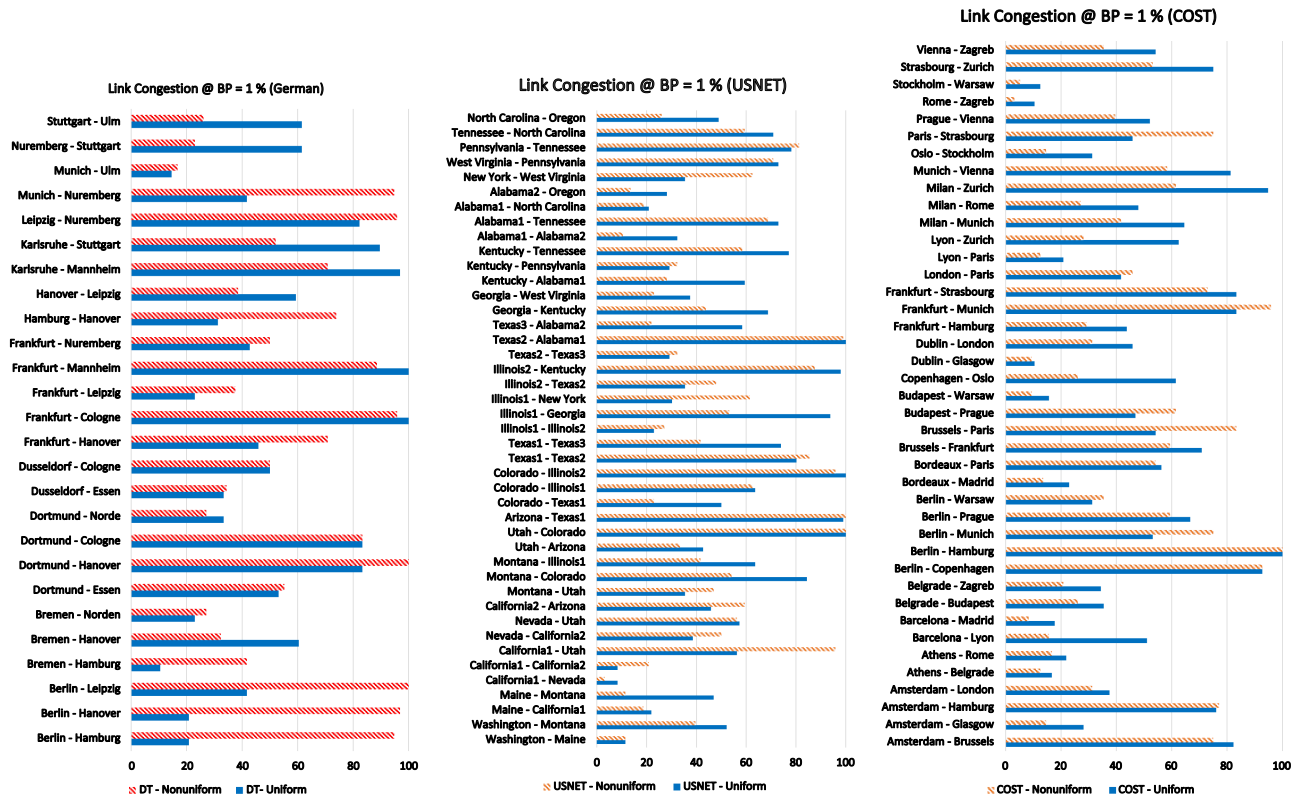

Fig. 11. Link congestion for the C-band scenario with BP $= 10^{-2}$ for (a) German, (b) US-NET, and (c) COST topology.

7. CONCLUSION

We have proposed a strategy to control multiband WDM line systems and enable BDM upgrades to C-band transmission as an alternative to the currently employed SDM approach. We considered C+L-band and C+L+S-band solutions with cardinalities of 2, 3, and 4 and proposed the implementation of a multiband power control scheme for maximizing and flattening the per-span GSNR by optimizing the amplifier gain and tilt. Results obtained by brute-force optimization showed significant improvement both in GSNR average and flatness with respect to the simple per-band LOGO strategy. Specifically, the optimized C+L-band transmission practically doubled the C-band's capacity, whereas the two C+L+S-band solutions showed limited impact on C+L bands, while enabling poorer yet acceptable GSNR on the S-band, at least for short distance connections.

We then applied the optimized transmission to perform a statistical network performance assessment on three network topologies with an increasing geographical footprint, i.e., the German, COST, and US-NET networks, each loaded according to two different traffic models: uniform and nonuniform proportional to the population. Results showed that the BDM solutions always enable a large traffic upgrade with a multiplication factor that does not exceed the upgrade cardinality, except for three cases. The network assessment was performed by also assuming SDM upgrades that are based on replications of C-band line systems. Comparing the results of BDM to SDM highlights that SDM solutions only slightly outperform those of BDM, confirming BDM to be a cost-effective and pay-as-you-need solution to upgrade networks without installing new cables. We also presented a link-congestion analysis, displaying how larger geographical footprint topologies suffer from blocking due to local traffic; this can be solved by BDM upgrades that exploit poorer QoT bands such as the S-band for local traffic, all the while using C+L-band transmission for longer reach traffic.

Funding. H2020 Marie Skłodowska-Curie Actions (814276).

REFERENCES

1. K. Kim, K. Doo, H. H. Lee, S. Kim, H. Park, J. Oh, and H. S. Chung, "High speed and low latency passive optical network for 5G wireless systems," J. Lightwave Technol. **37**, 2873–2882 (2019).
2. H. Yuan, M. Furdek, A. Muhammad, A. Saljoghei, L. Wosinska, and G. Zervas, "Space-division multiplexing in data center networks: on multi-core fiber solutions and crosstalk-suppressed resource allocation," J. Opt. Commun. Netw. **10**, 272–288 (2018).
3. L. Zhang, J. Chen, E. Agrell, R. Lin, and L. Wosinska, "Enabling technologies for optical data center networks: spatial division multiplexing," J. Lightwave Technol. **38**, 18–30 (2020).
4. J. Pedro, N. Costa, and S. Pato, "Optical transport network design beyond 100 Gbaud [Invited]," J. Opt. Commun. Netw. **12**, A123–A134 (2020).
5. P. S. Khodashenas, J. M. Rivas-Moscoso, D. Siracusa, F. Pederzolli, B. Shariati, D. Klonidis, E. Salvadori, and I. Tomkos, "Comparison of spectral and spatial super-channel allocation schemes for SDM networks," J. Lightwave Technol. **34**, 2710–2716 (2016).

6. F. Pederzolli, D. Siracusa, B. Shariati, J. M. Rivas-Moscoso, E. Salvadori, and I. Tomkos, "Improving performance of spatially joint-switched space division multiplexing optical networks via spatial group sharing," J. Opt. Commun. Netw. **9**, B1–B11 (2017).
7. A. Ferrari, A. Napoli, J. K. Fischer, N. Costa, A. D'Amico, J. Pedro, W. Forysiak, E. Pincemin, A. Lord, A. Stavdas, J. P. F. P. Gimenez, G. Roelkens, N. Calabretta, S. Abrate, B. Sommerkorn-Krombholz, and V. Curri, "Assessment on the achievable throughput of multi-band ITU-T G.652.D fiber transmission systems," J. Lightwave Technol. **38**, 4279–4291 (2020).
8. M. Klinkowski, P. Lechowicz, and K. Walkowiak, "A study on the impact of inter-core crosstalk on SDM network performance," in *International Conference on Computing, Networking and Communications (ICNC)* (IEEE, 2018), pp. 404–408.
9. A. Napoli, N. Costa, J. K. Fischer, J. Pedro, S. Abrate, N. Calabretta, W. Forysiak, E. Pincemin, J. P. Gimenez, C. Matrakidis, G. Roelkens, and V. Curri, "Towards multiband optical systems," in *Advanced Photonics 2018 (BGPP, IPR, NP, NOMA, Sensors, Networks, SPPCom, SOF)*, Washington, DC (Optical Society of America, 2018), paper NeTu3E.1.
10. A. Ferrari, A. Napoli, J. K. Fischer, N. Costa, J. Pedro, N. Sambo, E. Pincemin, B. Sommerkohrn-Krombholz, and V. Curri, "Upgrade capacity scenarios enabled by multiband optical systems," in *International Conference on Transparent Optical Networks*, July 2019, pp. 3–6.
11. S. Okamoto, K. Horikoshi, F. Hamaoka, K. Minoguchi, and A. Hirano, "5-band (O, E, S, C, and L) WDM transmission with wavelength adaptive modulation format allocation," in *European Conference on Optical Communication (ECOC)* (2016), pp. 20–22.
12. A. Arnould, A. Ghazisaeidi, H. Mardoyan, P. Brindel, M. Ionescu, and J. Renaudier, "High-speed and ultra-wideband devices for coherent transmission: challenges and opportunities," in *22nd International Conference on Transparent Optical Networks (ICTON)* (2020).
13. A. Ferrari, E. Virgillito, and V. Curri, "Band-division vs. space-division multiplexing: a network performance statistical assessment," J. Lightwave Technol. **38**, 1041–1049 (2020).
14. D. Semrau, E. Sillekens, R. I. Killey, and P. Bayvel, "The benefits of using the S-band in optical fiber communications and how to get there," in *IEEE Photonics Conference (IPC)* (IEEE, 2020).
15. M. Ionescu, D. Lavery, A. Edwards, E. Sillekens, D. Semrau, L. Galdino, R. I. Killey, W. Pelouch, S. Barnes, and P. Bayvel, "74.38 tb/s transmission over 6300 km single mode fibre enabled by C+L amplification and geometrically shaped PDM-64QAM," J. Lightwave Technol. **38**, 531–537 (2020).
16. M. Cantono, R. Schmogrow, M. Newland, V. Vusirikala, and T. Hofmeister, "Opportunities and challenges of C+L transmission systems," J. Lightwave Technol. **38**, 1050–1060 (2019).
17. A. Ferrari, D. Pilori, E. Virgillito, and V. Curri, "Power control strategies in C+L optical line systems," in *Optical Fiber Communications Conference and Exhibition (OFC)* (2019), paper W2A.48.
18. E. Virgillito, R. Sadeghi, A. Ferrari, G. Borraccini, and V. Curri, "Network performance assessment of C+L upgrades vs. fiber doubling SDM solutions," in *Optical Fiber Communication Conference (OFC)*, Washington, DC (OSA, 2020), paper M2G.4.
19. E. Virgillito, R. Sadeghi, A. Ferrari, A. Napoli, B. Correia, and V. Curri, "Network performance assessment with uniform and non-uniform nodes distribution in C+L upgrades vs. fiber doubling SDM solutions," in *International Conference on Optical Network Design and Modelling (ONDM)* (2020).
20. I. Roberts, J. M. Kahn, J. Harley, and D. W. Boertjes, "Channel power optimization of WDM systems following Gaussian noise nonlinearity model in presence of stimulated Raman scattering," J. Lightwave Technol. **35**, 5237–5249 (2017).
21. V. Lopez, B. Zhu, D. Moniz, N. Costa, J. Pedro, X. Xu, A. Kumpera, L. Dardis, J. Rahn, and S. Sanders, "Optimized design and challenges for C&L band optical line systems," J. Lightwave Technol. **38**, 1080–1091 (2020).
22. F. Hamaoka, M. Nakamura, S. Okamoto, K. Minoguchi, T. Sasai, A. Matsushita, E. Yamazaki, and Y. Kisaka, "Ultra-wideband WDM transmission in S-, C-, and L-bands using signal power optimization scheme," J. Lightwave Technol. **37**, 1764–1771 (2019).
23. M. Cantono, D. Pilori, A. Ferrari, C. Catanese, J. Thouras, J.-L. Augé, and V. Curri, "On the interplay of nonlinear interference generation with stimulated Raman scattering for QOT estimation," J. Lightwave Technol. **36**, 3131–3141 (2018).
24. M. Filer, M. Cantono, A. Ferrari, G. Grammel, G. Galimberti, and V. Curri, "Multi-vendor experimental validation of an open source QOT estimator for optical networks," J. Lightwave Technol. **36**, 3073–3082 (2018).
25. V. Curri, M. Cantono, and R. Gaudino, "Elastic all-optical networks: a new paradigm enabled by the physical layer. How to optimize network performances?" J. Lightwave Technol. **35**, 1211–1221 (2017).
26. J. Renaudier, A. Arnould, A. Ghazisaeidi, D. L. Gac, P. Brindel, E. Awwad, M. Makhsiyan, K. Mekhazni, F. Blache, A. Boutin, L. Letteron, Y. Frignac, N. Fontaine, D. Neilson, and M. Achouche, "Recent advances in 100+nm ultra-wideband fiber-optic transmission systems using semiconductor optical amplifiers," J. Lightwave Technol. **38**, 1071–1079 (2020).
27. V. Curri, "Software-defined WDM optical transport in disaggregated open optical networks," in *22nd International Conference on Transparent Optical Networks (ICTON)* (2020).
28. E. London, E. Virgillito, A. D'Amico, A. Napoli, and V. Curri, "Simulative assessment of non-linear interference generation within disaggregated optical line systems," OSA Continuum **3**, 3378–3389 (2020).
29. A. Ferrari, M. Filer, K. Balasubramanian, Y. Yin, E. Le Rouzic, J. Kundrát, G. Grammel, G. Galimberti, and V. Curri, "GNPy: an open source application for physical layer aware open optical networks," J. Opt. Commun. Netw. **12**, C31–C40 (2020).
30. "GitHub repository of GNPy," https://github.com/Telecominfraproject/oopt-gnpy.
31. J. Bromage, "Raman amplification for fiber communications systems," J. Lightwave Technol. **22**, 79–93 (2004).
32. R. Pastorelli, S. Piciaccia, G. Galimberti, E. Self, M. Brunella, G. Calabretta, F. Forghieri, D. Siracusa, A. Zanardi, E. Salvadori, G. Bosco, A. Carena, V. Curri, and P. Poggiolini, "Optical control plane based on an analytical model of non-linear transmission effects in a self-optimized network," in *39th European Conference and Exhibition on Optical Communication (ECOC)* (2013).
33. V. Curri, A. Carena, A. Arduino, G. Bosco, P. Poggiolini, A. Nespola, and F. Forghieri, "Design strategies and merit of system parameters for uniform uncompensated links supporting Nyquist WDM transmission," J. Lightwave Technol. **33**, 3921–3932 (2015).
34. P. Poggiolini, G. Bosco, A. Carena, R. Cigliutti, V. Curri, F. Forghieri, R. Pastorelli, and S. Piciaccia, "The LOGON strategy for low-complexity control plane implementation in new-generation flexible networks," in *Optical Fiber Communication Conference (OFC)* (2013), paper OW1H.3.
35. Fiberlabs Inc. AMP-FL8221-SB-16 amplifier datasheet.
36. J. Pedro and S. Pato, "On scaling transport networks for very high nodal degree ROADM nodes using state-of-the-art optical switch technology," in *17th International Conference on Transparent Optical Networks (ICTON)* (2015).